Dynamics at the Protein-Water Interface from ^{17}O Spin Relaxation in Deeply Supercooled Solutions

Carlos Mattea, Johan Qvist, and Bertil Halle
Center for Molecular Protein Science, Department of Biophysical Chemistry, Lund University, Lund, Sweden

ABSTRACT Most of the decisive molecular events in biology take place at the protein-water interface. The dynamical properties of the hydration layer are therefore of fundamental importance. To characterize the dynamical heterogeneity and rotational activation energy in the hydration layer, we measured the ^{17}O spin relaxation rate in dilute solutions of three proteins in a wide temperature range extending down to 238 K. We find that the rotational correlation time can be described by a power-law distribution with exponent 2.1–2.3. Except for a small fraction of secluded hydration sites, the dynamic perturbation in the hydration layer is the same for all proteins and does not differ in any essential way from the hydration shell of small organic solutes. In both cases, the dynamic perturbation factor is <2 at room temperature and exhibits a maximum near 262 K. This maximum implies that, at low temperatures, the rate of water molecule rotation has a weaker temperature dependence in the hydration layer than in bulk water. We attribute this difference to the temperature-independent constraints that the protein surface imposes on the water H-bond network. The free hydration layer studied here differs qualitatively from confined water in solid protein powder samples.

INTRODUCTION

The biological functions of most proteins depend critically on the dynamical properties of the protein-water interface. It is therefore of fundamental importance to obtain a quantitative description of water dynamics in the hydration layer enveloping the protein. Many experimental techniques have been applied to this problem, but our understanding is still incomplete (1). Studies of protein hydration dynamics are challenging for several reasons. First, few techniques can probe water molecules selectively. Second, at physiologically relevant hydration levels, the measured property tends to be dominated by the large excess of bulk water. Third, the mobility of water molecules varies by orders of magnitude among different hydration sites on the structurally heterogeneous protein surface.

Oxygen-17 spin relaxation has been used extensively to study single-molecule rotation in bulk water (2,3) and in the hydration shells of small organic solutes (4,5) and proteins (1,6,7) in dilute aqueous solution. In the case of protein solutions, frequency-dependent ^{17}O magnetic relaxation dispersion (MRD) measurements allow detailed characterization of internal water molecules (6,8), but provide only limited information about the rapidly exchanging water molecules in the external hydration layer (1,7). Essentially, the ^{17}O spin relaxation rate R_1 at high resonance frequency ($\sim$100 MHz) yields the average rotational correlation time $\langle\tau\rangle$ for all water molecules in the hydration layer, often reported as the dynamic perturbation factor (DPF) $\xi_H = \langle\tau\rangle/\tau_0$, where τ_0 is the bulk-water correlation time. (The DPF is sometimes called the rotational retardation factor (1).) Because of the topographical and chemical heterogeneity of the protein surface, the τ-distribution ranges from picoseconds to nanoseconds (1,9,10). In principle, information about this distribution could be obtained from measurements of the intermolecular cross-relaxation between water protons and spectrally resolved protons on the protein surface (11). However, because the cross-relaxation rate is usually dominated by long-range dipole couplings to remote bulk-water protons (7,12), this approach has not provided useful information about dynamics in the protein hydration layer.

Our principal aim here is to use ^{17}O spin relaxation to elucidate the generic dynamical behavior of the protein hydration layer in the presence of excess bulk water. Current magnet technology sets an upper limit of $\sim$100 MHz for the ^{17}O resonance frequency, so the picosecond-nanosecond hydration layer dynamics cannot be resolved directly in the frequency domain, as for internal water molecules (8). Our strategy is instead to characterize the dynamically heterogeneous hydration layer via the temperature dependence of the ^{17}O spin relaxation rate at a fixed high frequency. For this strategy to be effective, measurements must be performed over a wide temperature range. High temperatures are precluded by thermal denaturation and dominant internal water contributions to the ^{17}O relaxation rate even at high frequencies. On the low temperature side, water freezing presents an obstacle. However, by dispersing the protein solution in the form of emulsion droplets, the (metastable) liquid state can be maintained down to the homogeneous nucleation temperature (13,14). We have thus studied dilute solutions of three proteins in a 50 K temperature range extending down to 238 K. Accurate relaxation measurements in the deeply supercooled regime are technically challenging and until recently such data were not available even for small

Submitted April 11, 2008, and accepted for publication June 5, 2008.

Address reprint requests to Bertil Halle, E-mail: bertil.halle@bpc.lu.se.

Carlos Mattea's present address is Institute of Physics, Technical University of Ilmenau, Ilmenau D-98684, Germany.

Editor: Arthur G. Palmer 3rd.

0006-3495/08/09/2951/13 $2.00

doi: 10.1529/biophysj.108.135194

organic solutes (5). For small solutes, the data can be analyzed in a straightforward and essentially model-independent way. For proteins, data analysis is complicated by the strong dynamical heterogeneity. Before presenting the experimental results, we therefore outline the theoretical framework needed to analyze this kind of data.

The three proteins studied here, bovine pancreatic trypsin inhibitor (BPTI), ubiquitin, and β-lactoglobulin (BLG), were selected because they do not undergo cold denaturation in the investigated temperature range and because results from previous MRD studies (8,15) of the long-lived internal water molecules in these proteins allow us to reliably correct for the (small) contribution from internal water molecules to R_1 at high frequencies.

MATERIALS AND METHODS

Sample preparation

Bovine pancreatic trypsin inhibitor (BPTI, batch 9104, 97% purity by HPLC) from Bayer HealthCare AG (Wuppertal, Germany) was exhaustively dialyzed to remove residual salt. Ubiquitin was expressed in *Escherichia coli* and was purified to >99% as described (8). Bovine β-lactoglobulin (BLG) isoform A (cat. No. L-7880; Sigma, St. Louis, MO) was purified by anion exchange and size-exclusion chromatography as described in Qvist et al. (15). Protein solutions were prepared by dissolving the purified lyophilized protein in ^{17}O-enriched H_2O (19 atom % ^{17}O; Isotec, St. Louis, MO) and adjusting pH to the desired value (Table 1). Protein concentrations, expressed as the water/protein mole ratio N_W (Table 1), were determined with ~1% accuracy by complete amino-acid analysis. Nuclear magnetic resonance (NMR) measurements were made down to 238 K on emulsions of protein solution in heptane, with sorbitan tristearate as emulsifier (5). In a typical emulsion droplet of 10 μm diameter, only 0.3% of the protein molecules in the solution are within 5 nm of the interface. Furthermore, polyols (like the sorbitan headgroup of the emulsifier) are preferentially excluded from protein surfaces, so the protein should not interact strongly with the interface. Indeed, no effect of the interface could be detected in control experiments where ^{2}H and ^{17}O MRD profiles (1–100 MHz) were recorded at temperatures above 277 K from identical BPTI (16) or β-lactoglobulin (M. Davidovic, C. Mattea, J. Qvist, and B. Halle, unpublished) solutions with and without confinement to emulsion droplets.

Spin relaxation measurements

The relaxation rate R_1 of the water ^{17}O longitudinal magnetization was measured at 81.3 MHz on a Varian Unity Plus 600 spectrometer (Varian Cary, Palo Alto, CA). R_1 was determined with 0.5–1.0% accuracy from a three-parameter fit to the single-exponential magnetization curve obtained with the inversion recovery pulse sequence with 30 delay times in nonmonotonic order. The small scatter indicated that no freezing occurred during relaxation measurements down to 238 K. Reported R_1 values are averages of several measurements. At each temperature, measurements of R_1^0 on a pure water reference sample were alternated with solution R_1 measurements. The samples were carefully equilibrated at each temperature, which was regulated to within 0.1 K with a precooled stream of dry air and determined before and after R_1 measurements with a copper-constantan thermocouple in an NMR tube containing a water-ethanol mixture.

TABLE 1 Sample characteristics and results derived from ^{17}O relaxation data

Property	BPTI	Ubiquitin	BLG
M_P (kDa)	6.5	8.6	18.4
$\tau_P(T^*)$ (ns)	3.9	4.8	11.0
C_P (mM)	9.46	5.10	0.98
pH	5.2	5.0	2.7
N_W	5590	10500	55730
N_H	380	443	735
ν	2.32 ± 0.02	2.32 ± 0.01	2.15 ± 0.01
E_H^-(kJ mol^{-1})	26.5 ± 0.5	27.3 ± 0.3	27.0 ± 0.3
$T_X(p = 1)$	263.1	261.6	261.0
$T_X(p = 0.5$ or $0.9)$	264.1	262.4	263.0

Hydration numbers

The number of water molecules in the first hydration layer around the protein was computed as $N_H = A_S/a_W$, where A_S is the solvent-accessible surface area (SASA) of the protein and a_W is the amount of SASA occupied by one water molecule on average. The SASA was computed with GetArea 1.1 (17), using 1.7 Å probe radius and standard van der Waals radii (18). We used the value $a_W = 10.75$ Å^2, established for peptides and other organic solutes (5) by requiring that the SASA-derived hydration number N_H matches the hydration number computed from a molecular dynamics (MD) simulation as the mean number of water molecules satisfying at least one of the following criteria: $R(O_W–O) < 3.3$ Å; $R(O_W–N) < 3.5$ Å; and $R(O_W–C) < 5.0$ Å. These cutoff distances are close to the first minimum in the radial distribution function (19). Averaging over 2000 configurations from a 4-ns MD trajectory of BLG at $N_W = 6249$ (15), we obtain with the same cutoff distances $N_H = 745 \pm 13$, close to $A_S/a_W = 7906/10.75 = 735$. This agreement indicates that the adopted a_W value is valid for proteins as well as for small organic solutes. Previous MRD studies of protein hydration have used $a_W = 15$ Å^2 (1,20), leading to smaller N_H values that agree with MD simulations when a uniform cutoff $R(O_W–X) < 3.5$ Å is used to define the hydration layer (21). However, this more conservative definition of the hydration layer excludes most of the water in the primary hydration shells of apolar groups. The value $a_W = 10.75$ Å^2 adopted here yields N_H values that correspond more closely to the first layer of water molecules covering the protein. Note that the previously used a_W value of 15 Å^2 yields a somewhat larger DPF since the observed effect is attributed to a smaller number of water molecules. The DPF can be converted between the different a_W conventions according to $\xi_H^{new} = 1+(10.75/15)\,(\xi_H^{old} - 1)$.

THEORY

Water ^{17}O spin relaxation in protein solutions

The water ^{17}O spin relaxation rate R_1 in a protein solution exceeds the bulk-water value R_1^0 because the water molecules that interact with the protein rotate more slowly. The exceptionally high cohesive energy density of liquid water, stemming from the small size and fourfold hydrogen-bonding capacity of the water molecule, essentially limits the range of the protein-induced perturbation to the first hydration layer (and to the few water molecules that penetrate the protein). Support for this view comes from NMR relaxation studies of model systems (22,23) and from MD simulations (21,24). (Note that, in MD simulations, the first hydration shell of apolar groups is sometimes included in the second hydration layer of the protein (21,25).)

Accordingly, we attribute the observed relaxation enhancement to the N_H water molecules in the first hydration layer (Table 1) and to the N_I internal water molecules. The

^{17}O spin relaxation rate $R_1(\omega_0,T)$ for a protein solution with water/protein mole ratio N_W can then be expressed as (6)

$$R_1(\omega_0,T)=\left(1-\frac{N_H+N_I}{N_W}\right)R_1^0(T)+\frac{N_H}{N_W}\langle R_1^H(\omega_0,T)\rangle + \frac{N_I}{N_W}\langle \hat{R}_1^I(\omega_0,T)\rangle, \quad (1)$$

where $R_1^0(T)$ is the ^{17}O spin relaxation rate for a pure-water reference sample.

In the second term, the angular brackets represent an average over the N_H sites in the hydration layer. The form of this term assumes that all hydration sites are in the fast-exchange limit, which is the case at the high resonance frequency used here, $\omega_0/(2\pi)=81.3$ MHz. The intrinsic relaxation rate at a given hydration site is

$$R_1^H(\omega_0,T)=\omega_Q^2[0.2J_H(\omega_0,T)+0.8J_H(2\omega_0,T)], \quad (2)$$

where ω_Q is the ^{17}O nuclear quadrupole frequency. The spectral density function,

$$J_H(\omega,T)=\int_0^\infty dt\cos(\omega t)G_H(t,T), \quad (3)$$

is the cosine transform of the time correlation function (TCF),

$$G_H(t,T)=\exp\left[-\left(\frac{1}{\tau_P(T)}+\frac{1}{\tau(T)}\right)t\right], \quad (4)$$

where τ_P is the rotational correlation time of the protein (Table 1) and τ is the rotational correlation time of a water molecule in the hydration site. This form of the TCF follows from the statistical independence of protein tumbling and water motions in the hydration layer.

The third term in Eq. 1 describe the contribution to R_1 from N_I internal water molecules. Here, we do not assume fast exchange but only dilute conditions ($N_I \ll N_W$). The effective average intrinsic relaxation rate for the internal-water class is (6)

$$\langle \hat{R}_1^I(\omega_0,T)\rangle=\frac{1}{N_I}\sum_{k=1}^{N_I}\frac{1}{\tau_k^I(T)+1/R_{1,k}^I(\omega_0,T)}, \quad (5)$$

where τ_k^I is the mean water residence time in internal site k. The intrinsic relaxation rate $R_{1,k}^I(\omega_0,T)$ is given by expressions analogous to Eqs. 2–4, except that the TCF is now

$$G_k^I(t,T)=(S_k^I)^2\exp\left[-\left(\frac{1}{\tau_P(T)}+\frac{1}{\tau_k^I(T)}\right)t\right], \quad (6)$$

where S_K^I is the orientational order parameter of a water molecule in site k (6).

By measuring R_1 for a protein solution and R_1^0 for a pure-water reference sample at the same temperature, we can obtain the apparent dynamic perturbation factor (ADPF), defined as

$$\xi(\omega_0,T)\equiv 1+\frac{N_W}{N_H}\left[\frac{R_1(\omega_0,T)-R_1^0(T)}{R_1^0(T)}\right], \quad (7)$$

where N_W is the water/protein mole ratio in the sample and N_H is the number of water molecules in the hydration layer (Table 1). By substituting $R_1(\omega_0,T)$ from Eq. 1, we can express the ADPF as a sum of two terms associated with the hydration layer and with internal water molecules:

$$\xi(\omega_0,T)=\xi_H(\omega_0,T)+\xi_I(\omega_0,T). \quad (8)$$

These terms are given by

$$\xi_H(\omega_0,T)=\frac{\langle R_1^H(\omega_0,T)\rangle}{R_1^0(T)} = \frac{1}{\tau_0(T)}[0.2\langle J_H(\omega_0,T)\rangle+0.8\langle J_H(2\omega_0,T)\rangle], \quad (9)$$

$$\xi_I(\omega_0,T)=\frac{N_I}{N_H}\left[\frac{\langle \hat{R}_1^I(\omega_0,T)\rangle}{R_1^0(T)}-1\right]. \quad (10)$$

Our aim here is to study the hydration-layer ADPF $\xi_H(\omega_0,T)$, so we minimize the internal-water contribution $\xi_I(\omega_0,T)$ by measuring R_1 at a high resonance frequency, $\omega_0/(2\pi)=81.3$ MHz. The remaining small $\xi_I(\omega_0,T)$ contribution was computed from Eq. 10 with known parameter values (8,15). After this minor correction, we thus obtain $\xi_H(\omega_0,T)$ from the experimental data. The central problem, which we now address, is to interpret the temperature dependence of $\xi_H(\omega_0,T)$.

Dynamic heterogeneity in the hydration layer

The angular brackets in Eq. 9 signify an average over the temperature-dependent distribution $f(\tau,T)$ of correlation times τ in the hydration layer. To calculate this average, we need to know the mathematical form of the distribution function $f(\tau,T)$. From previous MRD studies (1,7), we know that the longest water correlation times in the hydration layer are in the nanosecond range at room temperature. The shortest correlation times, at exposed hydration sites, should be similar to the bulk-water correlation time of ~2 ps at room temperature. The correlation time distribution is therefore very wide, spanning three orders of magnitude. The precise functional form of the distribution has not been determined experimentally, but the MRD data (1,7) require it to be highly skewed toward shorter τ-values, with only a small number of hydration sites in the nanosecond range. This limited experimental information is consistent with the more detailed results of molecular dynamics (MD) simulations (9,10,26,27). The simulations indicate that the distribution of correlation times in the hydration layer of proteins can be described by a power law. We therefore adopt the power-law form

$$f(\tau,T)=C(T)\tau^{-\nu}, \quad (11)$$

where $C(T)$ is a normalization constant and the exponent ν is assumed to be independent of temperature, as indicated by MD simulations (9).

At a given temperature, the correlation times of the $N_H=380$–735 water molecules (Table 1) in the hydration layer fall

in a broad but finite range: $\tau_-(T) \leq \tau \leq \tau_+(T)$. Within this temperature-dependent range, the correlation times are taken to be distributed according to Eq. 11. Outside this range, $f(\tau,T) = 0$. We must now specify the limits of the distribution. From previous MRD studies (1,6,7,28) and MD simulations (9,10,21,24,26,27,29–31) of protein solutions and from studies of the hydration dynamics of small organic solutes (5,32–35), we know that, at room temperature, the lower limit τ_- is close to the bulk-water correlation time τ_0 and that the upper limit τ_+ is a few nanoseconds. As a natural choice for the upper limit, we choose the protein tumbling time τ_P, which is in the nanosecond range for the investigated proteins (Table 1). This choice is not critical, because the averages in Eq. 9 are quite insensitive to the upper limit τ_+ (Appendix A). This is so because 1), the power-law distribution is highly skewed toward shorter correlation times; and 2), protein tumbling acts to filter-out longer correlation times (see Eq. 4). We introduce a reference temperature T^*, where these limits apply. This temperature should be close to room temperature and we choose the temperature $T^* = 293.2$ K, where many of the previous studies have been performed. At this temperature, $\tau_0 = 1.8$ ps (2,3). At the reference temperature, we thus have

$$\tau_-(T^*) = \tau_0(T^*) \text{ and } \tau_+(T^*) = \tau_P(T^*). \quad (12)$$

To obtain the distribution $f(\tau,T)$ at an arbitrary temperature T, we must know how the limits $\tau_-(T)$ and $\tau_+(T)$ vary with temperature. From ^{17}O spin relaxation measurements on supercooled bulk water, we know the temperature dependence of τ_0 (2,3). Furthermore, the protein tumbling time τ_P is known to scale as $\eta_0(T)/T$ (36) and the temperature dependence of the bulk-water viscosity η_0 is known (37). At low temperatures, and especially in the supercooled regime, both τ_0 and η_0 exhibit an anomalously strong (super-Arrhenius) temperature dependence, caused by interference with the cooperative rotation mechanism (38) as the bulk liquid structure becomes more open and tetrahedrally ordered, that is, more icelike (39). However, in the hydration layer, the fixed (temperature-independent) geometric and H-bonding constraints imposed by the protein surface prevent the structural changes responsible for the anomalous temperature dependence of bulk-water dynamics. We therefore expect water dynamics in the hydration layer to exhibit a weaker, more normal (Arrhenius-like) temperature dependence than in bulk water. This has recently been shown to be the case for peptides and other small organic solutes (5). We thus assume that the temperature dependence of the shortest and longest water correlation time in the protein hydration layer follow the Arrhenius law, but with different activation energies and preexponential factors. (Note that it is not necessary to assume that all water molecules in the hydration layer follow the Arrhenius law.) The limits of the power-law distribution, given by Eq. 12 at T^*, then vary with temperature as

$$\tau_\pm(T) = A_\pm \exp\left[E_H^\pm/(k_B T)\right]. \quad (13)$$

Since the upper limit $\tau_+(T)$ is unimportant (see above), the effect of the assumed Arrhenius law essentially enters via the lower limit $\tau_-(T)$. We have tested Eq. 13 by analyzing the relaxation data with an extended model, where the activation energy E_H^- is allowed to depend linearly on temperature. The results indicate that Eq. 13 is an excellent approximation in the investigated temperature range (Appendix A).

The width of the correlation time range is essentially determined by the activation energies E_H^- and E_H^+, rather than by the preexponential factors A_- and A_+. In other words: $|\ln(A_+/A_-)| \ll \ln[\tau_+(T^*)/\tau_-(T^*)]$ so that Eqs. 12 and 13 yield

$$E_H^+ - E_H^- = k_B T^* \ln\left[\frac{\tau_P(T^*)}{\tau_0(T^*)}\right]. \quad (14)$$

The model thus contains only two free parameters, which we choose as ν and E_H^-.

Averaging the TCF in Eq. 4 over the correlation time distribution in Eq. 11, we obtain

$$\langle G_H(t,T)\rangle = C(T)\exp\left[-\frac{t}{\tau_P(T)}\right]\frac{1}{t^{\nu-1}} \times [\Gamma(\nu-1, t/\tau_-(T)) - \Gamma(\nu-1, t/\tau_+(T))], \quad (15)$$

with the incomplete γ-function defined as

$$\Gamma(a,t) \equiv \int_0^t dx\, e^{-x} x^{a-1}. \quad (16)$$

The hydration-layer-averaged spectral density function in Eq. 9 can now be obtained from Eqs. 3 and 13–15. The protein tumbling time $\tau_P(T)$ in Eq. 15 is obtained from experimentally determined values at T^* (Table 1) and the hydrodynamic $\eta_0(T)/T$ scaling (36). In general, the cosine transform in Eq. 3 must be evaluated numerically, but for the special case $\nu = 2$ we obtain the simple analytical result

$$\langle J_H(\omega,T)\rangle = \frac{1}{2}\left[\frac{1}{\tau_-^P(T)} - \frac{1}{\tau_+^P(T)}\right]^{-1} \ln\left\{\frac{1+\left[\omega\tau_-^P(T)\right]^{-2}}{1+\left[\omega\tau_+^P(T)\right]^{-2}}\right\}, \quad (17)$$

where

$$\tau_\pm^P(T) \equiv \left[\frac{1}{\tau_\pm(T)} + \frac{1}{\tau_P(T)}\right]^{-1}. \quad (18)$$

At high frequencies and low temperatures, where $(\omega\tau_-^P)^2 \ll 1$, $(\omega\tau_+^P)^2 \gg 1$, and $\tau_- \ll \tau_+, \tau_p$, Eq. 17 reduces to

$$\langle J_H(\omega,T)\rangle = -\tau_-(T)\ln[\omega\tau_-(T)]. \quad (19)$$

Substitution of this result into Eq. 9 yields for the ADPF

$$\xi_H(\omega_0,T) = \frac{\tau_-(T)}{\tau_0(T)}\ln[2^{4/5}\omega_0\,\tau_-(T)]^{-1}. \quad (20)$$

Once the model parameters ν and E_H^- have been determined from a fit to the experimental $\xi_H(\omega_0,T)$, we can calculate the

temperature variation of the mean correlation time $\langle\tau\rangle$ and the true DPF $\xi_H(T) \equiv \langle\tau\rangle/\tau_0$. We can also calculate these quantities for subpopulations, such as the 50% most mobile water molecules in the hydration layer. To calculate the partial DPF $\xi_H(T,p)$, we need the average correlation time $\langle\tau(T,p)\rangle$ for the fraction p of hydration sites with shortest correlation times. For the power-law distribution in Eq. 11, we obtain

$$\langle\tau(T,p)\rangle = \begin{cases} \dfrac{1}{p}\left[\dfrac{1}{\tau_-(T)} - \dfrac{1}{\tau_+(T)}\right]^{-1} \ln\left[\dfrac{\tau_p(T)}{\tau_-(T)}\right], \nu = 2 \\ \dfrac{1}{p}\left(\dfrac{\nu-1}{\nu-2}\right)\left\{\dfrac{[\tau_-(T)]^{2-\nu} - [\tau_p(T)]^{2-\nu}}{[\tau_-(T)]^{1-\nu} - [\tau_+(T)]^{1-\nu}}\right\}, \nu \neq 2 \end{cases}, \quad (21)$$

with

$$\tau_p(T) = \tau_-(T)\left\{1 - p + p\left[\frac{\tau_-(T)}{\tau_+(T)}\right]^{\nu-1}\right\}^{-1/(\nu-1)}. \quad (22)$$

For $p = 1$ (the entire hydration layer), Eq. 22 reduces to $\tau_p(T) = \tau_+(T)$. If $\tau_+ \gg \tau_-$, Eq. 21 yields for $\nu = 2$ and $p = 1$,

$$\langle\tau(T)\rangle = \tau_-(T)\ln\left[\frac{\tau_+(T)}{\tau_-(T)}\right]. \quad (23)$$

For this case, the effective activation energy of $\langle\tau(T)\rangle$ becomes

$$\overline{E}_H \equiv -k_B T^2 \frac{d\ \ln\langle\tau(T)\rangle}{dT} = E_H^- + k_B T, \quad (24)$$

where we have used Eq. 13.

A related, but more general, result can be obtained if we assume that the correlation times at all hydration sites obey the Arrhenius law with the same preexponential factor but with different activation energies. The power-law τ-distribution in Eq. 11 then corresponds to an exponential distribution of activation energies in the range $E_H^- \le E_H \le E_H^+$,

$$g(E_H,T) = D(T)\exp\left[-\frac{(\nu-1)}{k_B T}E_H\right], \quad (25)$$

with the normalization constant $D(T)$. From this distribution, we can calculate the mean activation energy for the hydration layer. For $\tau_+ \gg \tau_-$, we obtain the simple result

$$\langle E_H(T)\rangle \equiv \int_0^\infty dE_H\, g(E_H,T)\, E_H = E_H^- + \frac{k_B T}{\nu - 1}, \quad (26)$$

which coincides with Eq. 24 for $\nu = 2$.

EXPERIMENTAL RESULTS

For dilute aqueous solutions of the three proteins BPTI, ubiquitin, and β-lactoglobulin (BLG), we have measured the water ^{17}O spin relaxation rate $R_1(\omega_0,T)$ at a resonance frequency of 81.3 MHz and in a 50 K temperature range extending down to 238 K. At each temperature, we also measured the relaxation rate R_1^0 or a pure-water reference sample. To prevent the samples from freezing, the aqueous phase was dispersed as $\sim$10 μm-sized droplets in an emulsion (13). Because of the extremely strong temperature dependence of water dynamics at these low temperatures (2,3), high-precision relaxation measurements and careful temperature control are required (see Materials and Methods) to extract the hydration-layer dynamics from the small difference between R_1 and R_1^0.

The measured R_1 is an average over all rapidly exchanging water molecules in the sample, comprising bulk water, hydration water (in direct contact with the protein surface), and internal water (buried in cavities inside the protein). The contributions from these water classes, described by the three terms in Eq. 1, are shown in Fig. 1 for the ubiquitin sample. The internal-water contribution, which is very small, was calculated (at the experimental temperatures) from Eqs. 1–6 with parameter values from Table 1 and Persson and Halle (8). The bulk-water contribution was obtained from the relaxation rate R_1^0 measured on a pure-water reference sample, using N_W and N_H values from Table 1. Finally, the hydration-layer contribution was obtained by subtracting the internal-water and bulk-water contributions from the relaxation rate R_1 measured on the protein solution. The data in Fig. 1 show 1), that the hydration-layer contribution is an order-of-magnitude smaller than the bulk-water contribution at a protein concentration of 5 mM; and 2), that, at low temperatures, the hydration-layer contribution has a weaker temperature dependence than the bulk-water contribution.

For a quantitative comparison of the temperature dependencies of the hydration-layer and bulk-water contributions, we focus on their ratio, that is, on the apparent dynamic perturbation factor (ADPF) for the hydration layer, $\xi_H(\omega_0,T)$, defined in Eq. 9. This quantity is obtained by subtracting the small (negligible at low temperatures) internal-water contribution $\xi_I(\omega_0,T)$ from the total ADPF $\xi(\omega_0,T)$, obtained from the measured $R_1(\omega_0,T)$ and R_1^0 values by means of Eq. 7. The internal-water contribution is calculated with the aid of Eqs.

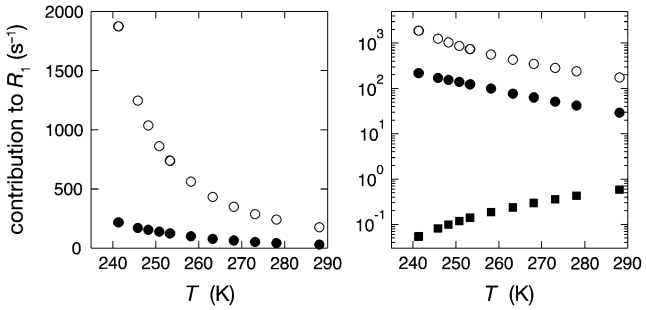

FIGURE 1 Temperature dependence of different contributions to the water ^{17}O relaxation rate R_1 at 81.3 MHz for a 5.1 mM ubiquitin solution at pH 5.0, plotted on linear (*left*) and logarithmic (*right*) scales. The depicted R_1 contributions correspond to the three terms in Eq. 1, representing 10,000 bulk water molecules (○), 443 water molecules in the hydration layer (●), and a single internal water molecule (■).

2, 3, 5, 6, and 10. For this calculation, we need to know, for each internal site, the order parameter S_k^I and the residence time τ_k^I. For BPTI, these quantities have been determined for all four internal water molecules at the reference temperature T^* (8). The order parameters are governed by the protein structure and should therefore be essentially independent of temperature. The temperature dependence of the residence times is described by activation energies that have been determined experimentally (8). For ubiquitin ($N_I = 1$) and BLG ($N_I = 3$), the internal-water contribution is negligibly small at all investigated temperatures. Nevertheless, this small contribution was computed from the known or estimated internal-water parameters (8,15) and subtracted from the total ADPF.

The measured total ADPF and its hydration-layer and internal-water contributions, separated as described above, are shown in Fig. 2 for the three proteins. Evidently, the internal-water contribution (*dark shaded area*) is significant only for BPTI, and then only at the higher temperatures. The dominant hydration-layer ADPF $\xi_H(\omega_0,T)$ (*light shaded area*) exhibits a broad maximum at 267–271 K for the three proteins. Such a maximum has not been observed previously for proteins. The $\xi_H(\omega_0,T)$ curves in Fig. 2 were obtained from fits where the two free parameters in the model were adjusted: the exponent ν in the power-law correlation time distribution (Eq. 11) and the activation energy E_H^- at the short-τ end of the distribution (Eq. 13). The resulting parameter values are given in Table 1. The exponent ν has the same value for BPTI and ubiquitin. The slightly smaller value for BLG implies a broader τ-distribution, consistent with an unusually large (but still $\ll 1$) fraction of hydration sites with long correlation times (comparable to, or longer than, $1/\omega_0$). This conclusion is consistent with the observation of an unusually strong frequency dependence in the 10–100 MHz range of the room-temperature MRD profile of BLG (15). The minimum activation energy E_H^- is 27 kJ mol^{-1} for all three proteins. From Eq. 14, we obtain $E_H^+ = 45$, 46, and 48 kJ mol^{-1} for BPTI, ubiquitin, and BLG, respectively. From Eq. 26, we obtain for all three proteins $\langle E_H(T^*)\rangle = 28$ kJ mol^{-1} at the reference temperature $T^* = 293.2$ K. The fitted values of ν and E_H^- are insensitive to reasonable variations in $\tau_-(T^*)$ and $\tau_+(T^*)$ (Appendix A).

From the model parameters ν and E_H^-, we can calculate the temperature variation of the true (rather than apparent) DPF $\xi_H(T)$, which relates hydration-layer dynamics to bulk-water dynamics in an essentially method-independent and model-independent way. The temperature dependence of the DPF $\xi_H(T)$ exhibits a maximum at 262 ± 1 K for all three proteins (Table 1, Fig. 3, *left panel*). Formally,

$$\frac{d\xi_H(T)}{dT} = \frac{\xi_H(T)}{k_B T^2}[E_0(T) - \overline{E}_H(T)], \tag{27}$$

where E_0 and $\overline{E}_H$ are the apparent Arrhenius activation energies of τ_0 and $\langle\tau\rangle$, respectively, defined as in Eq. 24. The DPF maximum thus occurs at the crossover temperature T_X where the weakly temperature-dependent (Eq. 24) activation energy $\overline{E}_H$ of the mean hydration-layer correlation time $\langle\tau\rangle$ matches the strongly temperature-dependent activation energy E_0 of the bulk-water correlation time τ_0:

$$E_0(T_X) = \overline{E}_H(T_X). \tag{28}$$

The reduction of $\xi_H(T)$ at lower temperatures is thus primarily caused by the drastic slowing down of bulk-water motions. The ADPF curves (Fig. 2) do not differ much from the DPF curves (Fig. 3, *left panel*), suggesting that the reason for the reduction of $\xi_H(\omega_0,T)$ at low temperatures is the same as for $\xi_H(T)$.

At first sight, one might be tempted to interpret the ADPF maxima in Fig. 2 in terms of a maximum in the spectral density function $\tau/[1+(\omega_0\tau)^2]$ with increasing correlation time τ. However, this cannot be the case because nearly all water molecules in the hydration layer have subnanosecond correlation times even at the lowest investigated temperature. Furthermore, if this explanation were correct, then $\langle R_1^H(\omega_0,T)\rangle$ would exhibit a maximum, which is not the case (Fig. 1). The frequency dependence in $\langle R_1^H(\omega_0,T)\rangle$ reduces the magnitude of $\xi_H(\omega_0,T)$ and shifts the temperature of its maximum slightly, but it does not give rise to the $\xi_H(\omega_0,T)$ maximum. This frequency dependence explains why the difference between the ADPF curves in Fig. 2 and the DPF curves in Fig. 3 (*left panel*) is largest for BLG, which contains the largest fraction hydration sites with correlation times of order $1/\omega_0$ or longer (15). This fraction of relatively slow hydration sites also accounts for the substantially larger maximum DPF for BLG (7.4) as compared to BPTI (4.7) and ubiquitin (4.9) in Fig. 3 (*left panel*). (The experimentally determined power-law exponent ν is close to 2, where equal intervals of $\log(\tau)$ make equal contributions to $\langle\tau\rangle$.)

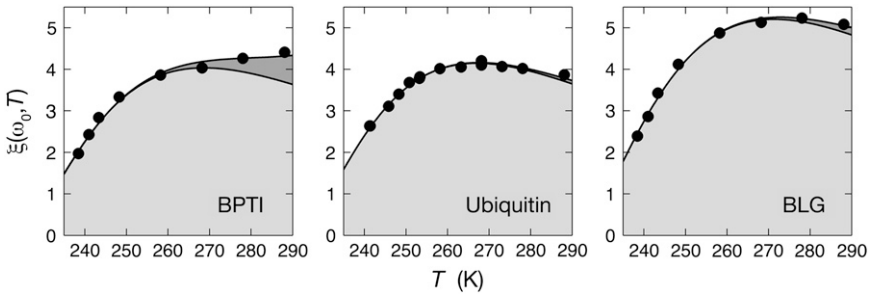

FIGURE 2 Temperature dependence of the ADPF $\xi(\omega_0,T)$ at 81.3 MHz for BPTI, ubiquitin, and BLG. The contributions from hydration water (*light shading*) and internal water (*dark shading*) are indicated. The curves were obtained by fitting the two model parameters ν and E_H^- (Table 1) to the data (*solid circles*).

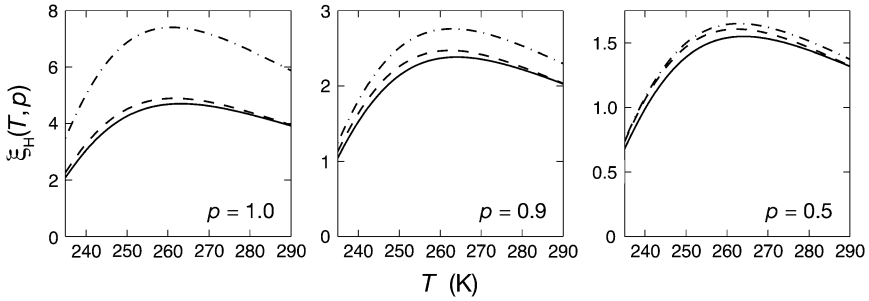

FIGURE 3 Temperature dependence of the hydration-layer DPF $\xi_H(T,p)$ for BPTI (*solid curves*), ubiquitin (*dash*), and BLG (*dash-dot*). The three panels show the DPF for all N_H hydration waters (*left*), the 90% most mobile waters (*middle*), and the 50% most mobile waters (*right*).

From the model parameters ν and E_H^-, we can also calculate the partial DPF $\xi_H(T,p)$ for the most mobile fraction p of the N_H water molecules in the hydration layer (Eq. 21). Whereas the DPF can be strongly affected by a minor fraction of protein-specific hydration sites, the partial DPF for the 90 or 50% most mobile water molecules in the hydration layer should reflect the generic dynamics for most of the hydration layer. Although based on only three proteins, the convergence of the 50% DPF curves (Fig. 3, *right panel*) supports this view.

The different temperature dependence of bulk and hydration water dynamics is displayed in the form of an Arrhenius plot in Fig. 4. Whereas the τ_0 curve is strongly curved (super-Arrhenius temperature dependence), the $\langle\tau\rangle$ curves are nearly linear. The high degree of linearity is to some extent a result of assuming that $\tau_-(T)$ obeys the Arrhenius law (Eq. 13), since for a broad distribution (with $\tau_+ \gg \tau_-$), $\langle\tau\rangle$ is approximately proportional to $\tau_-(T)$ (Eq. 23). However, the data in Fig. 2 demonstrate in a model-independent way that the activation energy has a weaker temperature dependence for $\langle\tau\rangle$ than for τ_0. Moreover, three-parameter fits to the data in Fig. 2 allowing for a linear temperature dependence in E_H^- show that this dependence is insignificant (Appendix A). The data do not uniquely determine the functional form of the distribution $f(\tau,T)$, but they are consistent with a power-law distribution. Given this functional form, the data indicate that the temperature dependence of $\langle\tau\rangle$ does not deviate much from the Arrhenius law in the range 238–288 K, where τ_0 deviates strongly (Fig. 4).

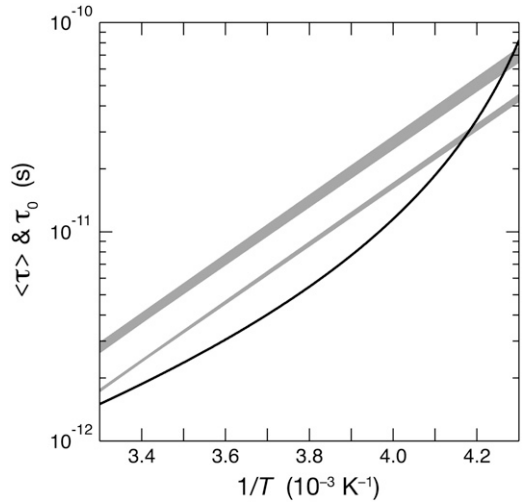

FIGURE 4 Arrhenius plot showing the mean correlation time $\langle\tau\rangle$ for the 50% (*narrow shaded band*) and 90% (*wide shaded band*) most mobile hydration waters and the correlation time τ_0 in bulk water (*solid curve*). The shaded bands each contain three nearly linear curves for BPTI, ubiquitin, and BLG.

DISCUSSION

Proteins versus peptides

The DPF at 300 K has been determined previously from the MRD profiles for the three proteins studied here and several others (1,20). Extrapolating the curves in Fig. 3 (*left panel*) to 300 K, we find ξ_H values of 3.6 for BPTI and ubiquitin, and 5.3 for BLG, consistent with previous results (15,40). The mean and standard deviation for 11 monomeric proteins was reported as $\xi_H = 1 + (0.30 \pm 0.04)\, a_W$ (1). For the mean solvent-accessible area occupied per water molecule, $a_W = 10.75$ Å^2, adopted here (see Materials and Methods), this yields $\xi_H = 4.2 \pm 0.4$.

To what extent, and why, does the hydration layer differ from one protein to another? The majority of the several hundred water molecules that constitute the hydration layer of a protein are associated with convex protrusions on the surface and only a minority of the hydration waters occupy concave depressions or pockets on the protein surface. It is in the latter, more secluded, locations that we find the water molecules with the longest correlation times (1,10,26,27). The substantial variation of the full DPF $\xi_H(T, p = 1)$ among different proteins (Fig. 3, *left panel*) reflects protein-specific variations in the relative abundance of such secluded hydrations sites. The convergence of the partial DPFs $\xi_H(T, p)$ as the secluded hydrations sites are removed from the average ($p = 1 \rightarrow 0.9 \rightarrow 0.5$) suggests that the remaining major part of the hydration layer has the same average dynamics for most proteins (Fig. 3, *middle* and *right panels*).

Disregarding the protein-specific small subset of secluded hydration sites, does the dominant generic part of the protein hydration layer differ dynamically from the hydration shell of small organic solutes? The hydration structure of a small apolar solute (like methane) differs from that at a flat apolar

surface (41), but solvent-exposed protein surfaces are not flat on the scale of a water molecule. Water NMR relaxation data over a wide temperature range have recently been reported for dilute aqueous (D_2O) solutions of two small peptides: N-acetyl-glycine-N′-methylamide (NAGMA) and N-acetyl-leucine-N′-methylamide (NALMA) (5). Such small solutes do not contain the type of secluded hydration sites that are responsible for the long-τ tail of the τ-distribution for the protein hydration layer. Therefore, we have $\omega_0\tau \ll 1$ for all hydration sites at all investigated temperatures and $\xi_H(\omega_0,T) = \xi_H(T)$ (Eq. 9). We thus obtain the DPF $\xi_H(T)$ without having to specify the form of the correlation time distribution $f(\tau,T)$. (As explained in the Theory section, this is not possible for proteins.) Just as for the proteins studied here, NAGMA and NALMA yield a maximum in $\xi_H(T)$. The observation of a $\xi_H(T)$ maximum for small solutes supports our conclusion that the $\xi_H(\omega_0,T)$ maximum observed here for proteins is caused by a crossover of activation energies rather than by a R_1 maximum associated with correlation times of order $1/\omega_0$. For all three proteins, we obtain $T_X = 263 \pm 1$ K for $p = 0.9$ and for $p = 0.5$ (Table 1, Fig. 3, *middle* and *right panels*), only 7 K above the T_X value for the peptides (5). The maximum ξ_H (at T_X) is 1.55 for NAGMA and 2.40 for the more hydrophobic NALMA (5). Very similar maximum ξ_H values are obtained for the proteins: 2.38 (1.55), 2.47 (1.61), and 2.76 (1.65) for BPTI, ubiquitin, and BLG, respectively, at $p = 0.9$ (0.5). From the similar ξ_H and T_X values obtained for proteins and peptides, we conclude that the dynamics, and presumably also the structure, at the vast majority of protein hydration sites are essentially the same as in the hydration shell of small peptides (and other organic solutes (5)). The only essential difference between protein and small-solute hydration is the presence of a minority of secluded hydration sites on protein surfaces, responsible for the long-τ tail of the correlation time distribution.

The similar hydration dynamics of proteins and small solutes was noted in previous work from this laboratory (1,7), but the limited amount of temperature-dependent NMR relaxation data available at that time did not allow a quantitative comparison. While previously published low-temperature MRD profiles for BPTI (7) are consistent with the present findings, the nonmonotonic temperature dependence of the DPF was not anticipated. Instead, the observed ADPF reduction at low temperatures (for BPTI) was attributed to the gradual removal (when τ becomes comparable to $1/\omega_0$) of the contribution to the ADPF from a few strongly perturbed water molecules in secluded hydration sites. That this is not the main reason for the ADPF reduction at low temperatures is demonstrated by the present finding of a similar reduction of the DPF for three proteins (Fig. 3, *left panel*) and by similar results for four small organic solutes (5). Therefore, the previous conclusion (1,7) that $\langle\tau\rangle$, for most of the protein hydration layer, has a significantly weaker temperature dependence than $\langle\tau\rangle$ for the hydration shell of small organic solutes must be revised. A quantitative comparison with low-temperature data for small organic solutes, not available until recently (5), reveals that the hydration dynamics of proteins and small solutes depend on temperature in essentially the same way (see below).

Dynamical heterogeneity in the protein hydration layer

The correlation time τ probed by spin relaxation is closely related to the mean residence time (MRT) of a water molecule in a hydration site. In exposed sites with short τ-values, the water molecule is more strongly coupled to water than to protein. Rotation (τ) and translation (MRT) should then occur on the same timescale, since they are both governed by rearrangement of water-water H-bonds (1,30,42). In secluded sites with long τ-values, the water molecule is more strongly coupled to protein than to water. Rotation is then hindered (that is, only librations are allowed) until the water molecule is released by the protein so, again, τ should be close to the MRT.

Two MD simulation studies have reported the MRT distribution for the protein hydration layer; in both cases, the power-law distribution in Eq. 11 was found to describe the MRT data over a wide range (9,10). For cytochrome *c* (9), the exponent $\nu \approx 2.3$ (for the range 1 ps−1 ns) at 300 K agrees closely with our results (Table 1). (Since the data shown in Fig. 6 of García and Hummer (9) were not corrected for logarithmic binning, the slope yields $\nu - 1$; G. Hummer, National Institute of Diabetes and Digestive and Kidney Diseases, National Institutes of Health, personal communication, 2007.) The smaller exponent, $\nu = 0.84$ (for the range ~20 ps−20 ns), obtained for acetylcholinesterase (10) may reflect a broader τ-distribution for this 60 kDa protein, or it may simply be a consequence of the particular definition of time-averaged hydration sites used in that study (10).

Rotational correlation times are ideal for probing the dynamics in the hydration layer since rotation is a localized motion. In contrast, translational motion is inherently nonlocal, making it difficult to uniquely define a translational diffusion coefficient for the hydration layer. It is sometimes asserted that water diffusion in the hydration layer is anomalous in the sense that $\langle(\Delta r)^2\rangle \sim t^\alpha$ with $\alpha < 1$ (29,31). For a continuous-time random walk with a power-law waiting time distribution, as in Eq. 11, one can show that $\alpha = \nu - 1$ (43). However, the subdiffusive (for $\alpha < 1$) motion in this model results from the scale invariance of an unrestricted (valid for all τ) power-law distribution, leading to a divergent $\langle\tau\rangle$. In contrast, in the protein hydration layer, the τ values are limited to a finite range $[\tau_-, \tau_+]$. Furthermore, a water molecule that starts out in the hydration layer will rarely visit more than a few hydration sites before reaching the bulk water region. The α-exponents <1 deduced from MD simulations (29,31) may thus be artifacts of treating an inhomogeneous system as homogeneous, rather than being an indication of a fundamental change in the diffusion mechanism.

The spin relaxation rate R_1 reports on an orientational TCF $\langle G_H(t)\rangle$ that is averaged over all hydration sites on the heterogeneous protein surface. After the ubiquitous subpicosecond damped librational oscillation, the TCF $G_H(t)$ for a given hydration site should decay in an approximately exponential fashion, as in Eq. 4. However, because of the broad correlation time distribution, the average TCF decays nonexponentially, as seen from Eq. 15. In simulation studies, the average TCF is sometimes fitted (in a limited time interval) to a stretched exponential function, $\langle G_H(t)\rangle = \exp[-(t/\tau_S)^{\beta}]$ (24,29). The correlation time distribution $f(\tau)$ obtained by inverting this empirical function (44) does not exhibit the algebraic long-τ tail indicated by our data (and by MD simulations). The β-exponent is reported to be $\sim$0.5 or larger (24,29). For $\beta = 0.5$, the distribution implied by the stretched exponential TCF has the form $f(\tau) \propto \exp[-\tau/(4\tau_S)]/\sqrt{\tau}$ (44), which is very different from a power-law. The stretched exponential function may provide a decent fit in a limited time interval, but it has no theoretical basis and it misses the protein-specific algebraic tail of the correlation time distribution (which is rarely sampled with sufficient statistical accuracy in MD simulations).

Temperature dependence of hydration dynamics

In our analysis, the observed temperature dependence of R_1 is attributed entirely to water dynamics. We thus assume that the protein structure is independent of temperature so that the number N_H of water molecules in the hydration layer is constant. At the low temperatures studied here, protein cold denaturation (45) is a potential complication. For proteins that are known to cold-denature, we have found that cold denaturation is accompanied by a characteristic increase in the ADPF $\xi(\omega_0,T)$ at low temperatures (M. Davidovic, C. Mattea, J. Qvist, and B. Halle, unpublished). Because this feature is not seen for the three proteins investigated here, we conclude that these proteins do not cold-denature down to 238 K. This conclusion is consistent with the finding that the solution structure of BPTI is virtually identical at 258 and 309 K (46).

BLG is predominantly dimeric at neutral pH, but the large net charge (+20) at pH 2.7 reduces the dimer fraction to $<$10% under our salt-free conditions (47). Since the dimer interface buries only 6% of the protein's SASA (48), dimerization should not produce a significant temperature dependence in N_H. Furthermore, we neglect the small contraction of the protein at low temperatures. The thermal expansivity of most proteins is $\sim 1 \times 10^{-4}\ K^{-1}$ (49). Over a 50 K temperature interval, the protein volume thus changes by $\sim$0.5%, so N_H changes by merely $(1.005)^{2/3} - 1 = 0.3\%$.

The Arrhenius-like temperature dependence of the average correlation time $\langle\tau\rangle$ for the protein hydration layer (Fig. 4) may seem inconsistent with the wide range of activation energies, from $E_H^- \approx 27\ kJ\ mol^{-1}$ to $E_H^+ \approx 47\ kJ\ mol^{-1}$, of the individual hydration sites on the protein surface. But the exponential E_H distribution decays with a characteristic energy of $k_BT/(\nu - 1)$ so that the activation energy of $\langle\tau\rangle$ is essentially $E_H^- + k_BT/(\nu - 1)$ (Eqs. 24–26), which differs little from E_H^-. In other words: whereas $\langle\tau\rangle$ has substantial contributions from the long-τ tail of the correlation time distribution, the temperature dependence of $\langle\tau\rangle$ is almost completely determined by the more numerous hydration sites with τ close to the lower limit τ_-. To understand the Arrhenius-like behavior of $\langle\tau\rangle$, we must thus explain why E_H^- is constant whereas the bulk-water activation energy E_0 varies strongly with temperature (2,3).

In bulk water, molecular rotation is a highly cooperative process where large energy barriers are circumvented by a concerted interchange of hydrogen-bonding partners (38,50,51). Decreasing temperature favors low-density configurations with high (icelike) tetrahedral order, which interfere with the cooperative rotation mechanism. This progressive structural change accounts for the dramatic increase of the apparent activation energy E_0 in supercooled bulk water. In the protein hydration layer, the slowing down of water rotation can also be attributed to interference with the cooperative rotation mechanism, partly because of the reduced number of nearby water molecules with which to swap H-bonds and partly because H-bond partners in the protein are either absent (at apolar sites) or else are geometrically constrained (at polar sites). Because these constraints are essentially temperature-independent, the activation energy E_H^- should not change much with temperature. In a sense, the hydration layer can be regarded as a defect in the surrounding, increasingly tetrahedrally ordered, supercooled solvent. At sufficiently low temperatures, we therefore expect most of the hydration layer to have higher mobility than bulk water. Indeed, our analysis predicts that $\langle\tau\rangle$ for the 50 and 90% most mobile hydration waters falls below τ_0 at 239 $\pm$ 1 K and 234 $\pm$ 1 K, respectively (Fig. 3). For the peptides NAGMA and NALMA, the corresponding temperature is 237 K (5). Thus, again we see that most of the water molecules in the protein hydration layer behave in the same way as water molecules in the hydration shell of small organic solutes.

Coupling of protein and water dynamics

The solvent plays a dual role by fundamentally altering the protein's conformational free energy landscape and by providing much of the thermal energy and frictional damping that together govern diffusive conformational motions in the protein. In addressing the latter dynamical aspect, the solvent may be modeled, to a first approximation, as a homogeneous viscous continuum. This description is implicit in conventional hydrodynamic treatments of global dynamics, domain movements, and protein folding.

At the next level of approximation, the dynamic perturbation of the solvent by the protein may be incorporated by assigning a local viscosity η_H to the hydration layer, different

from the bulk-water viscosity η_0 (36). In bulk water, the Stokes-Einstein-Debye radius is constant over a wide temperature range, demonstrating that molecular rotation samples dynamical heterogeneities in the same way as the viscosity (J. Qvist, C. Mattea, and B. Halle, unpublished). The rotational correlation time of hydration water is therefore a reasonable proxy for the local viscosity in the hydration layer (36). In other words: the ratio η_H/η_0 is essentially given by the DPF ξ_H. The relative importance of hydration layer and bulk water depends on the fraction of the viscous energy dissipation that occurs in each region. We therefore expect that the hydration layer is more important for localized motions than for large-scale motions and that it is more important for rotational motions than for translational motions (36). Our results show that most of the hydration layer is highly mobile, being retarded by a factor 2 or less (Fig. 3), as for the hydration shell of small organic solutes (5). While large-scale protein motions are only marginally affected by this perturbation (36), localized protein motions and ligand binding events that involve water displacement should be retarded to nearly the same extent as the hydration water. In view of the results in Fig. 4, we also expect that the frictional damping of localized protein motions has a weaker and more Arrhenius-like temperature dependence than if they were governed by bulk-water viscosity.

Free hydration layer versus confined water

In the protein solutions studied here, only 1–7% of the water molecules are in contact with the protein surface (Table 1). The water molecules in this free hydration layer interact with bulklike water as well as with the protein surface. Only by studying such dilute systems can we characterize the perturbation of bulk-water dynamics at the interface between liquid water and protein. Our results show that this perturbation has generic as well as protein-specific aspects (Fig. 3). This type of study represents a logical starting point for understanding protein-water interactions in vivo. It has been estimated that ~15% of the water in an *E. coli* cell belongs to the first hydration layer of proteins or other macromolecular structures (52). It is therefore likely that most solvent-exposed protein surfaces in vivo are surrounded by multiple water layers. As a model system, a dilute protein solution is thus not only well defined but also of direct biological relevance.

A substantial literature has accumulated on the study of protein-water interactions in solid samples at low water content, such as rehydrated protein powders (53,54). Such samples have been studied for their biotechnological relevance or simply because of the difficulty of separating the hydration-layer response from the dominant bulk-water background in a protein solution. Here, we want to caution against uncritical extrapolation of results obtained on solid water-poor samples to in vivo or dilute-solution conditions.

In a protein powder at a typical hydration level of 0.3 g H_2O (g protein)$^{-1}$, the protein molecules are densely packed at 70% volume fraction. For hen egg white lysozyme (HEWL), this water content corresponds to $N_W = 240$ or 40% of the 600 water molecules required to cover the protein surface (calculated as described in Materials and Methods). Some of the water molecules in this sample occupy subnanometer-sized interstitial spaces, others are buried in small cavities between contacting protein molecules. Few, if any, water molecules experience an environment that resembles a free hydration layer. Water dynamics in a protein powder may therefore be dominated by confinement effects and its temperature dependence may reflect structural and dynamic changes in the protein component more than intrinsic water dynamics.

These expectations are confirmed by a recent study of water diffusion (on a μm-length scale) in a HEWL powder sample with 0.3 g H_2O (g protein)$^{-1}$ (55). From the water self-diffusion coefficients measured in the powder sample (D_{powder}) and in bulk water (D_0), the DPF $\xi_{powder} = D_0/D_{powder}$ is found to vary from ~20 at 288 K to ~60 at 238 K (55). These values are 1–2 orders-of-magnitude larger than the DPF ξ_H for the free hydration layer (Fig. 3). (Note that the measured average diffusion coefficient D_{powder} is dominated by the most mobile water molecules, whereas the average correlation time $\langle\tau\rangle$ that we measure is biased toward the least mobile water molecules. This methodological difference should make ξ_{powder} smaller than ξ_H, not larger.) Furthermore, the diffusion coefficient D_{powder} was found to have an even more anomalous (super-Arrhenius) temperature dependence than the bulk-water diffusion coefficient D_0, so $\xi_{powder}(T)$ increases monotonically at least down to 238 K (55). In contrast, for the free hydration layer, we find that $\langle\tau\rangle$ has a much weaker temperature dependence than τ_0 (Fig. 4), resulting in a crossover of activation energies and a decrease of $\xi_H(T)$ at low temperatures (Fig. 3).

A series of recent studies indicate that water dynamics in a HEWL powder with 0.3 g H_2O (g protein)$^{-1}$ exhibit a weaker, Arrhenius-like temperature dependence to $<\sim$220 K (55–58). It was suggested (55–58) that this change in the temperature dependence of water dynamics triggers the glasslike dynamical transition that is observed in incompletely hydrated protein samples at 170–230 K and below which conformational fluctuations in the protein are suppressed (54,59,60). Moreover, it was proposed (56–58) that this transition has the same underlying cause as the apparent power-law singularity in bulk water properties at a similar temperature (61), namely a metastable liquid-liquid critical point in bulk water (62).

We are skeptical to these proposals. If water in protein powders differs qualitatively from the free hydration layer, why should it resemble bulk water? Although neither the apparent singularity nor the metastable low-temperature phase behavior of bulk water are understood, it is widely believed that these and other anomalies are linked to the tetrahedral H-bond network in liquid water. In a HEWL powder sample with 0.3 g H_2O (g protein)$^{-1}$, there is not

enough water to cover even half of the protein surface and few, if any, water molecules are likely to be fully coordinated by other water molecules. It is for this reason that water in protein powders does not form ice at any temperature; it remains in a thermodynamically stable state down to the glasslike dynamical transition. In contrast, bulk water, and the protein solutions studied here, are metastable with respect to ice I_h at subzero temperatures. Whereas the free hydration layer can be regarded as the perturbed interfacial region of a bulk liquid water phase, the water molecules in a protein powder do not participate in a bulklike H-bond network. In a protein powder, water and protein are so strongly coupled that it may be meaningless to say that either component triggers the dynamical transition, where water and protein motions are simultaneously suppressed.

CONCLUSIONS

The ^{17}O NMR relaxation data presented here provide a quantitative view of water dynamics in the hydration layer that constitutes the protein-water interface. Our main conclusions are as follows:

1. The strong dynamical heterogeneity of the protein hydration layer can be described by a power-law distribution of rotational correlation times, $f(\tau) \propto 1/\tau^{\nu}$, with exponent $\nu = 2.1$–2.3 for the three proteins examined here. The hydration-layer-averaged correlation time $\langle\tau\rangle$ obtained from the data thus has roughly equal contributions from equal logarithmic intervals within the broad τ-distribution.
2. The long-τ tail of the power-law distribution is associated with a protein-specific small population of slowly rotating water molecules, consistent with the finding from MD simulations that the most strongly perturbed water molecules reside in secluded sites (9,10,26,27).
3. The majority of the water molecules in the hydration layer exhibit a weak and generic (same for all proteins) dynamic perturbation. At room temperature, the average dynamic perturbation factor is $\sim$2 for 90% of the hydration layer and only $\sim$1.3 for the most mobile half of the layer.
4. At room temperature, the hydration-layer-averaged correlation time $\langle\tau\rangle$ has a stronger temperature dependence than the bulk-water correlation time τ_0, but at low temperatures the reverse is true. As a result, the dynamic perturbation factor $\xi_H = \langle\tau\rangle/\tau_0$ has a nonmonotonic temperature dependence, with a maximum at the crossover temperature $T_X = 262 \pm 1$ K where the apparent activation energies of hydration layer and bulk water are equal. Below 239 K, most water molecules in the hydration layer are more mobile than in bulk water.
5. The hydration layer can be regarded as a defect in the predominantly tetrahedrally coordinated H-bond network of bulk water, induced by a protein surface that provides fewer and less flexible H-bonding opportunities for the adjacent water molecules. These constraints slow down water rotation because they interfere with the cooperative mechanism that facilitates rotation in bulk water. Because the constraints are essentially temperature-independent, hydration water does not follow the strongly super-Arrhenius temperature dependence of bulk water. In this sense, hydration water is less anomalous than bulk water.
6. With the exception of a small fraction of secluded hydration sites, the protein hydration layer differs little from the hydration shell of peptides and other small organic solutes (5). In both cases, the dynamic perturbation factor is <2 at room temperature and exhibits a maximum near 260 K.
7. The free hydration layer at the protein-water interface differs fundamentally from confined water in partially hydrated solid protein samples, where the dynamic perturbation factor is 1–2 orders-of-magnitude larger and has a qualitatively different temperature dependence.

APPENDIX A

Robustness of model fit

The two free parameters ν and E_H^- in the model described in the Theory section were fitted to the relaxation data in Fig. 2. The resulting parameter values are given in Table 1. We also performed fits with different choices for the limits $\tau_-(T^*)$ and $\tau_+(T^*)$ of the correlation time distribution at the reference temperature T^*. The fit is insensitive to the upper limit. In particular, $\tau_+(T^*)$ can be increased without limit above $\tau_P(T^*)$ without affecting the fit, because R_1 depends on the effective correlation time $(1/\tau + 1/\tau_P)^{-1}$ rather than on τ itself (Eq. 4). The upper limit $\tau_+(T^*)$ can also be reduced from $\tau_P(T^*)$ by as much as a factor 4 without changing the parameters ν and E_H^- outside the error limits quoted in Table 1. The fit is more sensitive to the lower limit$\tau_-(T^*)$. Increasing or decreasing $\tau_-(T^*)$ by a factor 2 from $\tau_0(T^*)$ changes ν by 10–20% and E_H^- by 10–15%. Three-parameter fits, where $\tau_-(T^*)$ was also freely adjustable, gave $\tau_-(T^*)$ values well within this range.

To examine the temperature dependence of $\langle\tau\rangle$ in a less biased way, we removed the assumption of a strict Arrhenius temperature dependence for $\tau_-(T^*)$. (The temperature dependence of $\tau_+(T^*)$ is unimportant.) Specifically, we allowed the activation energy in Eq. 13 to depend on temperature according to $E_H^-(T) = E_H^-(260)[1+\sigma(260 - T)]$. We then performed three-parameter fits where ν, $E_H^-(260)$, and σ were adjusted. The values for ν and $E_H^-(260)$ differed by <0.02 and <0.4 kJ mol^{-1}, respectively, from the values given in Table 1. The temperature coefficient σ was not significantly different from zero for any of the three proteins. Taking the error limits into account, the fit indicates that $|\sigma| < 0.001$, corresponding to, at most, 5% variation of E_H^- over the examined 50 K interval.

We thank Hanna Nilsson for protein purification, Hans Lilja for NMR spectrometer maintenance, Erik Persson for NMR advice and discussions, and Bayer Healthcare AG for a generous supply of BPTI.

This work was supported by the Swedish Research Council, the Crafoord Foundation, and the Knut & Alice Wallenberg Foundation.

REFERENCES

1. Halle, B. 2004. Protein hydration dynamics in solution: a critical survey. *Philos. Trans. R. Soc. Lond. B Biol. Sci.* 359:1207–1224.

2. Hindman, J. C. 1974. Relaxation processes in water: viscosity, self-diffusion, and spin-lattice relaxation. A kinetic model. *J. Chem. Phys.* 60:4488–4496.
3. Lang, E. W., and H.-D. Lüdemann. 1982. Anomalies of liquid water. *Angew. Chem. Int. Ed. Engl.* 21:315–329.
4. Bagno, A., F. Rastrelli, and G. Saielli. 2005. NMR techniques for the investigation of solvation phenomena and non-covalent interactions. *Prog. Nucl. Magn. Reson. Spectrosc.* 47:41–93.
5. Qvist, J., and B. Halle. 2008. Thermal signature of hydrophobic hydration dynamics. *J. Am. Chem. Soc.* In press. DOI: 10.1021/ja802668w.
6. Halle, B., V. P. Denisov, and K. Venu. 1999. Multinuclear relaxation dispersion studies of protein hydration. *In* Biological Magnetic Resonance. N. R. Krishna, and L. J. Berliner, editors. Kluwer Academic/Plenum, New York.
7. Modig, K., E. Liepinsh, G. Otting, and B. Halle. 2004. Dynamics of protein and peptide hydration. *J. Am. Chem. Soc.* 126:102–114.
8. Persson, E., and B. Halle. 2008. Nanosecond to microsecond protein dynamics probed by magnetic relaxation dispersion of buried water molecules. *J. Am. Chem. Soc.* 130:1774–1787.
9. García, A. E., and G. Hummer. 2000. Water penetration and escape in proteins. *Proteins.* 38:261–272.
10. Henchman, R. H., and J. A. McCammon. 2002. Structural and dynamic properties of water around acetylcholinesterase. *Protein Sci.* 11:2080–2090.
11. Otting, G. 1997. NMR studies of water bound to biological molecules. *Prog. Nucl. Magn. Reson. Spectrosc.* 31:259–285.
12. Halle, B. 2003. Cross-relaxation between macromolecular and solvent spins: the role of long-range dipole couplings. *J. Chem. Phys.* 119: 12372–12385.
13. Rasmussen, D. H., and A. P. MacKenzie. 1973. Clustering in supercooled water. *J. Chem. Phys.* 59:5003–5013.
14. Angell, C. A. 1983. Supercooled water. *Annu. Rev. Phys. Chem.* 34: 593–630.
15. Qvist, J., M. Davidovic, D. Hamelberg, and B. Halle. 2008. A dry ligand-binding cavity in a solvated protein. *Proc. Natl. Acad. Sci. USA.* 105:6296–6301.
16. Jóhannesson, H., and B. Halle. 1998. Minor groove hydration of DNA in solution: dependence on base composition and sequence. *J. Am. Chem. Soc.* 120:6859–6870.
17. Fraczkiewicz, R., and W. Braun. 1998. Exact and efficient analytical calculation of the accessible surface areas and their gradients for macromolecules. *J. Comput. Chem.* 19:319–333.
18. Shrake, A., and J. A. Rupley. 1973. Environment and exposure to solvent of protein atoms. Lysozyme and insulin. *J. Mol. Biol.* 79:351–371.
19. Kim, B., T. Young, E. Harder, R. A. Friesner, and B. J. Berne. 2005. Structure and dynamics of the solvation of bovine pancreatic trypsin inhibitor in explicit water: a comparative study of the effects of solvent and protein polarizability. *J. Phys. Chem. B.* 109:16529–16538.
20. Denisov, V. P., and B. Halle. 1996. Protein hydration dynamics in aqueous solution. *Faraday Discuss.* 103:227–244.
21. Schröder, C., T. Rudas, S. Boresch, and O. Steinhauser. 2006. Simulation studies of the protein-water interface. I. Properties at the molecular resolution. *J. Chem. Phys.* 124:234907.
22. Woessner, D. E. 1980. An NMR investigation into the range of the surface effect on the rotation of water molecules. *J. Magn. Reson.* 39:297–308.
23. Carlström, G., and B. Halle. 1988. Water dynamics in microemulsion droplets. A nuclear spin relaxation study. *Langmuir.* 4:1346–1352.
24. Abseher, R., H. Schreiber, and O. Steinhauser. 1996. The influence of a protein on water dynamics in its vicinity investigated by molecular dynamics simulation. *Proteins.* 25:366–378.
25. Smolin, N., and R. Winter. 2004. Molecular dynamics simulations of Staphylococcal nuclease: properties of water at the protein surface. *J. Phys. Chem. B.* 108:15928–15937.
26. Makarov, V. A., B. K. Andrews, P. E. Smith, and B. M. Pettitt. 2000. Residence times of water molecules in the hydration sites of myoglobin. *Biophys. J.* 79:2966–2974.
27. Luise, A., M. Falconi, and A. Desideri. 2000. Molecular dynamics simulation of solvated azurin: correlation between surface solvent accessibility and water residence times. *Proteins.* 39:56–67.
28. Halle, B. 1998. Water in biological systems: the NMR picture. *In* Hydration Processes in Biology. M.-C. Bellisent-Funel, editor. IOS Press, Dordrecht, The Netherlands.
29. Bizzarri, A. R., and S. Cannistraro. 2002. Molecular dynamics of water at the protein-solvent interface. *J. Phys. Chem. B.* 106:6617–6633.
30. Marchi, M., F. Sterpone, and M. Ceccarelli. 2002. Water rotational relaxation and diffusion in hydrated lysozyme. *J. Am. Chem. Soc.* 124: 6787–6791.
31. Pizzitutti, F., M. Marchi, F. Sterpone, and P. J. Rossky. 2007. How protein surfaces induce anomalous dynamics of hydration water. *J. Phys. Chem. B.* 111:7584–7590.
32. Ishimura, M., and H. Uedaira. 1990. Natural abundance O-17 magnetic relaxation in aqueous solutions of apolar amino acids and glycine peptides. *Bull. Chem. Soc. Jpn.* 63:1–5.
33. Bagno, A., G. Lovato, G. Scorrano, and J. W. Wijnen. 1993. Solvation of nonelectrolytes in water probed by ^{17}O NMR relaxation of the solvent. *J. Phys. Chem.* 97:4601–4607.
34. Ishihara, Y., S. Okouchi, and H. Uedaira. 1997. Dynamics of hydration of alcohols and diols in aqueous solution. *J. Chem. Soc., Faraday Trans.* 93:3337–3342.
35. Shimizu, A., K. Fumino, K. Yukiyasu, and Y. Taniguchi. 2000. NMR studies on the dynamic behavior of water molecules in aqueous denaturant solutions at 25°C: effects of guanidine hydrochloride, urea and alkylated ureas. *J. Mol. Liq.* 85:269–278.
36. Halle, B., and M. Davidovic. 2003. Biomolecular hydration: from water dynamics to hydrodynamics. *Proc. Natl. Acad. Sci. USA.* 100: 12135–12140.
37. Hallett, J. 1963. The temperature dependence of the viscosity of supercooled water. *Proc. Phys. Soc.* 82:1046–1050.
38. Laage, D., and J. T. Hynes. 2006. A molecular jump mechanism of water reorientation. *Science.* 311:832–835.
39. Debenedetti, P. G. 2003. Supercooled and glassy water. *J. Phys. Cond. Mat.* 15:R1669–R1726.
40. Denisov, V. P., and B. Halle. 1995. Protein hydration dynamics in aqueous solution: a comparison of bovine pancreatic trypsin inhibitor and ubiquitin by oxygen-17 spin relaxation dispersion. *J. Mol. Biol.* 245: 682–697.
41. Chandler, D. 2005. Interfaces and the driving force of hydrophobic assembly. *Nature.* 437:640–647.
42. Geiger, A., M. Kleene, D. Paschek, and A. Rehtanz. 2003. Mechanisms of the molecular mobility of water. *J. Mol. Liq.* 106:131–146.
43. Klafter, J., G. Zumofen, and A. Blumen. 1993. Non-Brownian transport in complex systems. *Chem. Phys.* 177:821–829.
44. Lindsey, C. P., and G. D. Patterson. 1980. Detailed comparison of the Williams-Watts and Cole-Davidson functions. *J. Chem. Phys.* 73: 3348–3357.
45. Privalov, P. L. 1990. Cold denaturation in proteins. *Crit. Rev. Biochem. Biophys.* 25:281–305.
46. Shen, Y., and T. Szyperski. 2008. Structure of the protein BPTI derived with NOESY in supercooled water: validation and refinement of solution structures. *Angew. Chem. Int. Ed.* 47:324–326.
47. Sakurai, K., M. Oobatake, and Y. Goto. 2001. Salt-dependent monomer-dimer equilibrium of bovine β-lactoglobulin at pH 3. *Protein Sci.* 10:2325–2335.
48. Brownlow, S., J. H. M. Cabral, R. Cooper, D. R. Flower, S. J. Yewdall, I. Polikarpov, A. C. T. North, and D. W. Sawyer. 1997. Bovine β-lactoglobulin at 1.8 Å resolution—still an enigmatic lipocalin. *Structure.* 5:481–495.
49. Chalikian, T. V. 2003. Volumetric properties of proteins. *Annu. Rev. Biophys. Biomol. Struct.* 32:207–235.

50. Sciortino, F., A. Geiger, and H. E. Stanley. 1991. Effect of defects on molecular mobility in liquid water. *Nature*. 354:218–221.

51. Rodríguez Fris, J. A. R., G. A. Appignanesi, E. La Nave, and F. Sciortino. 2007. Metabasin dynamics and local structure in supercooled water. *Phys. Rev. E Stat. Nonlin. Soft Matter Phys.* 75:041501.

52. Persson, E., and B. Halle. 2008. Cell water dynamics on multiple time scales. *Proc. Natl. Acad. Sci. USA*. 105:6266–6271.

53. Rupley, J. A., and G. Careri. 1991. Protein hydration and function. *Adv. Protein Chem.* 41:37–172.

54. Gregory, R. B. 1995. Protein hydration and glass transition behavior. *In* Protein-Solvent Interactions. R. B. Gregory, editor. Marcel Dekker, New York.

55. Mallamace, F., S.-H. Chen, M. Broccio, C. Corsaro, V. Crupi, D. Majolino, V. Venuti, P. Baglioni, E. Fratini, C. Vannucci, and H. E. Stanley. 2007. Role of the solvent in the dynamical transitions of proteins: the case of the lysozyme-water system. *J. Chem. Phys.* 127: 045104.

56. Chen, S.-H., L. Liu, E. Fratini, P. Baglioni, A. Faraone, and E. Mamontov. 2006. Observation of fragile-to-strong dynamic crossover in protein hydration water. *Proc. Natl. Acad. Sci. USA*. 103:9012–9016.

57. Kumar, P., Z. Yan, L. Xu, M. G. Mazza, S. V. Buldyrev, S.-H. Chen, S. Sastry, and H. E. Stanley. 2006. Glass transition in biomolecules and the liquid-liquid critical point of water. *Phys. Rev. Lett.* 97:177802.

58. Lagi, M., X. Chu, C. Kim, F. Mallamace, P. Baglioni, and S.-H. Chen. 2008. The low-temperature dynamic crossover phenomenon in protein hydration water: simulations vs experiments. *J. Phys. Chem. B*. 112:1571–1575.

59. Daniel, R. M., R. V. Dunn, J. L. Finney, and J. C. Smith. 2003. The role of dynamics in enzyme activity. *Annu. Rev. Biophys. Biomol. Struct.* 32: 69–92.

60. Doster, W. 2008. The dynamical transition of proteins, concepts and misconceptions. *Eur. Biophys. J.* 37:591–602.

61. Speedy, R. J., and C. A. Angell. 1976. Isothermal compressibility of supercooled water and evidence for a thermodynamic singularity at −45°C. *J. Chem. Phys.* 65:851–858.

62. Poole, P. H., F. Sciortino, U. Essmann, and H. E. Stanley. 1992. Phase behavior of metastable water. *Nature*. 360:324–328.